Amyloid-β Oligomers Serve as Nucleation Sites for α-Synuclein Aggregation

Devkee M. Vadukul[1], Rebecca J. Thrush[1,2], Yiyun Jin[1] and Francesco A. Aprile[1,2]*
[1]Department of Chemistry, Molecular Sciences Research Hub, Imperial College London, London W12 0BZ, UK
[2]Institute of Chemical Biology, Molecular Sciences Research Hub, Imperial College London, London W12 0BZ, UK

*Author to whom correspondence should be addressed.
Email: f.aprile@imperial.ac.uk, Phone: +44 (0)20 7594 5545

Abstract
Neurodegenerative diseases are associated with the formation of amyloids in the nervous system. An increasing number of cases where amyloids of the same protein are found in different dementias is being reported. This observation complicates diagnosis and clinical intervention. Amyloids of the amyloid-β peptide or the protein α-synuclein are traditionally considered hallmarks of Alzheimer's and Parkinson's diseases, respectively. However, the co-occurrence of amyloids of these proteins has also been reported in patients diagnosed with either disease. Here, we provide new evidence about the protein composition of aggregates formed when these two proteins are co-present. We show that soluble species of amyloid-β can induce the aggregation of α-synuclein. The amyloid fibrils formed under these conditions are solely composed of α-synuclein to which amyloid-β can be found associated, but not as part of the core of the fibrils. Our data take us one step closer to understanding the complex nature of heterogenous aggregation in disease contexts which may aid clinical diagnosis and the development of therapeutic interventions.

Keywords: Alzheimer's disease, Parkinson's disease, co-aggregation, amyloid-β, α-synuclein

Introduction
Neurodegenerative diseases, including Alzheimer's (AD) and Parkinson's (PD) diseases, are characterized by the formation of fibrillar protein aggregates, called amyloids, in the nervous system (1). Amyloids are enriched in cross-β sheet and resistant to degradation (2, 3). In the case of AD, a key pathological hallmark are the extracellular amyloid plaques made of the amyloid-β peptide (Aβ) (4). Aβ exist as variants of different lengths (i.e., 38-49 residue-long) and originate by the proteolytic cleavage of the amyloid protein precursor (5-7). Aβ monomers undergo a self-assembly process that leads to the formation of amyloids via small transient intermediates, called oligomers (4). Thus far, Aβ monomers and amyloids are considered less pathogenic compared to the oligomers (8-11). Several toxic effects of Aβ oligomers have been identified, including inflammation, synaptotoxicity, membrane permeabilization and oxidative stress (8, 9, 12-19).

The co-occurrence of amyloids composed of Aβ and of other proteins has been detected in several neurodegenerative diseases, suggesting an interplay between Aβ and these amyloid forming proteins (20-26). One such protein is α-synuclein (α-syn), which is predominantly found as amyloid fibrils in Lewy bodies (LBs) in PD, Lewy body dementia, and Multiple System Atrophy (27-29). The identification of Aβ plaques in up to 50% of PD

patients (30, 31) and of LBs in almost 50% of AD patients (32) suggests a crosstalk between Aβ and α-syn. This hypothesis is further supported by the identification of the non-amyloid-β component (NAC) region of α-syn in AD plaques (32, 33).

The effects of Aβ and α-syn on each other's aggregations are not yet fully characterized at the molecular level. Recently, it has been found that α-syn can either accelerate or inhibit the aggregation of Aβ. This dual mechanism of α-syn has been observed on both the 40-residue-long (Aβ40) and the 42-residue-long (Aβ42) isoforms of Aβ (22, 34-38). Whether α-syn promotes or inhibits Aβ aggregation seems to depend on the aggregated state of α-syn. In fact, it has been shown that α-syn monomers can delay the aggregation of Aβ42, whilst α-syn amyloid fibrils can accelerate it (39). Conversely, it has been shown that Aβ42 is able to trigger the aggregation of α-syn (40). Furthermore, the formation of hetero-oligomers made of both Aβ42 and α-syn has been observed *in vitro*, suggesting that the two proteins can co-aggregate and form heterogeneous aggregates (41-43).

Here, we investigate the structures of the aggregates formed when Aβ42 and α-syn co-aggregate *in vitro*. Using a combination of biophysical and biochemical techniques, we report the presence of fibrillar aggregates, whose core is solely made of α-syn. Aβ42 is found to be associated to these fibrils, suggesting that it provides the hydrophobic surface required for α-syn to nucleate. Our findings take us one step closer to understanding the complex nature of heterogenous aggregation in disease contexts which may aid clinical diagnosis and the development of therapeutic strategies.

Results

Amyloid fibrils are formed in α-syn–Aβ42 co-incubation. To assess the effects of Aβ42 and α-syn on each other's aggregations, we carried out thioflavin T (ThT) assays on solutions containing 60 μM monomeric α-syn in the presence of a sub-stoichiometric concentration (2 μM) of monomeric Aβ42 (**Fig. 1**). Hereafter, we will refer to this condition as the co-incubation sample. As controls, we performed ThT experiments on solutions containing either 60 μM α-syn or 2 μM Aβ42. Under our experimental conditions, α-syn alone did not aggregate, while Aβ42 alone aggregated in approximately 4 h (**Fig. 1a**), as previously reported (44). When α-syn and Aβ42 were incubated together, the resulting aggregation was slower than that of Aβ42 alone. In particular, the aggregation half-time (t_{50}) of the co-incubation sample was approximately 1.7 times longer than that of Aβ42 alone (2.9 ± 0.35 and 1.7 ± 0.4 h, respectively) (**Fig. S1**).

To characterize the structures of the aggregates formed at the endpoint of aggregation, we carried out negative staining transmission electron microscopy (TEM) (**Fig. 1b and Fig. S2**). The electron micrographs confirmed that α-syn alone does not form visible aggregates. On the contrary, both Aβ42 only and the co-incubation sample contained fibrils. Analysis of the width of these fibrils revealed 25th and 75th percentiles of width distributions as 8/13 and 12/16 nm for Aβ42 and the co-incubation sample respectively (**Fig. 1c)**. The difference in fibril widths provided first insights that fibrils formed by co-incubation are likely not Aβ42 fibrils.

The fibrils formed in α-syn–Aβ42 co-incubation are made of α-syn. To investigate the protein composition of the aggregates, we performed immunogold TEM on samples collected at the aggregation endpoints (**Fig. 2a** and **Fig. S3**). To do so, the samples were simultaneously probed for Aβ42 with antibodies conjugated to 10 nm gold nanoparticles (Ab–10AuNPs) and α-syn with antibodies conjugated to 6 nm gold nanoparticles (Ab–6AuNPs). We found no or very low signal for Aβ42 in the sample with α-syn alone and for

α-syn in the samples with Aβ42 alone, verifying that our staining is specific (**Fig. S3**). The sample containing α-syn alone showed a diffuse distribution of small clusters of Ab–6AuNPs, confirming the presence of α-syn and the lack of fibrils (**Fig. S3c**), similarly to previous reports (40) and in agreement with our ThT and negative staining TEM data. The sample with Aβ42 contained fibrils decorated by Ab–10AuNPs, i.e., made of Aβ42 (**Fig. S3a**). Fibrils were also present in the co-incubation sample (**Fig. 2a**). However, similarly to our TEM analysis (**Fig. 1b and c**), these fibrils had a larger diameter than the fibrils of Aβ42 alone (**Fig. S3d**). Furthermore, they were predominantly decorated by 6Ab–AuNPs, i.e., made of α-syn. However, some Ab–10AuNPs could be detected on the fibrils as well, suggesting that Aβ42 was co-aggregated with α-syn.

Given that amyloid fibrils are SDS-insoluble, to assess whether Aβ42 was peripheral or within the core of the fibrils, we quantified Aβ42 and α-syn in the SDS-insoluble protein fraction at the aggregation endpoint. To do so, we washed the fibrils with SDS to remove any associated soluble aggregates and then treated the fibrils with guanidine hydrochloric acid (G-HCl). This was then analyzed by SDS-PAGE and western blotting (**Fig. 2b**). Detection with the anti-Aβ 6E10 antibody revealed that Aβ42 was present in the soluble and SDS-soluble fractions. On the other hand, α-syn was clearly detected by the anti-α-syn antibody in all pellet and supernatant fractions, including the G-HCl treated pellet. These results indicate that the fibrils formed under co-incubation are composed of only α-syn. While the immunogold labelled TEM showed some Aβ42 labelling (**Fig. 2a**), this is due to Aβ42 being associated to rather than within the core of the fibrils.

To further characterize the conformations of Aβ42 and α-syn after aggregation, we performed native-PAGE and western blotting on the endpoints of aggregation (**Fig. 2c**). We found that Aβ42 alone forms high molecular weight species that remain in the well of the gel, suggesting they are large fibrillar aggregates. Instead, α-syn alone is mainly monomeric as compared to freshly purified α-syn. In the co-incubation sample, more Aβ42 can enter the gel as compared to the Aβ42 alone condition. In particular, the protein forms high molecular weight species compatible with oligomers. In the co-incubation sample, α-syn is largely monomeric. However, it also forms high molecular weight species, some of which stay in the well of gel suggestive of fibrillar aggregates. While not all the α-syn aggregates in the presence of Aβ42, this is unsurprising and reminiscent of α-syn aggregation in the presence of lipids where the α-syn to lipid ratio is key in α-syn conversion during aggregation (45). Additionally, the same analysis of the samples at earlier time points showed that higher molecular weight assemblies of α-syn are not detected until Aβ42 oligomers are formed (**Fig. S4**). This further strengthens our hypothesis that it is the Aβ42 oligomers that are nucleating the aggregation of α-syn.

To better understand the solubility of Aβ42 and α-syn in co-incubation conditions, we carried out immuno-dot blots on the soluble protein fractions at the endpoints of aggregation (**Fig. S5**). Soluble Aβ42 and α-syn were detected using the 6E10 and anti-α-syn primary antibodies respectively and quantified by densitometry. Our data show that, when Aβ42 is incubated alone, there is a significant decrease in the amount of soluble Aβ42 by ~70% after aggregation when compared to freshly purified monomeric Aβ42. However, when Aβ42 is incubated with α-syn, the amount of soluble Aβ42 does not significantly change during aggregation. On the other hand, when α-syn is incubated alone, the protein remains largely soluble during the incubation; when compared to freshly purified α-syn, there is only a ~10% decrease in the amount of soluble protein. In the presence of Aβ42, the amount of soluble α-syn is further reduced by ~33%. This is in line with our observations that a small portion of α-syn aggregates in these co-incubation

conditions, however, the amount of aggregated insoluble protein represents only a small portion of the total α-syn.

Together, these data indicate that, in co-incubation conditions, Aβ42 is mainly in a soluble oligomeric conformation, while α-syn aggregates into amyloid fibrils. Furthermore, it is likely that the soluble Aβ42 found associated to α-syn fibrils are the nucleation site for α-syn aggregation due to their hydrophobic surface.

Aβ42 fibrils do not trigger the aggregation of α-syn. To assess whether α-syn aggregation is triggered by soluble or fibrillar Aβ42, we incubated 60 μM α-syn in the presence or absence of 2 μM pre-formed Aβ42 fibrils (**Fig. 3**). We measured the ThT fluorescence of samples containing α-syn alone, Aβ42 fibrils alone, and α-syn in the presence of Aβ42 fibrils (**Fig. 3a**). As expected, we observed that α-syn alone does not aggregate. Aβ42 fibrils alone have a steady ThT fluorescence as does the co-incubation sample. Immunogold TEM showed that the fibrils in the co-incubation sample are largely labelled with the Ab–10AuNPs specific for Aβ (**Fig. 3b** and **Fig. S6a**). This result confirms that there is no aggregation of α-syn and, conversely, that Aβ42 fibrils are not affected by soluble α-syn. Strengthening this observation, dot blot analysis on the soluble and insoluble protein fractions revealed that no soluble Aβ42 was present in the sample containing Aβ42 fibrils alone (**Fig. 3c and Fig. S6b**). Soluble Aβ42 was also not detected in the co-incubation sample confirming that α-syn had no effect on fibrillar Aβ42, which is in sharp contrast to the effect of incubating α-syn with soluble Aβ42. Additionally, no difference in the amount of soluble α-syn between the co-incubation and α-syn alone samples was detected (**Fig. 3c and Fig. S6c)**. Native-PAGE and western blotting on the endpoints of aggregation (**Fig. 3d**) revealed no soluble Aβ42 in the Aβ42 alone and co-incubation samples. No difference in the molecular weight of α-syn was observed in the α-syn alone and co-incubation samples. This evidence indicates that fibrillar Aβ42 does not affect the aggregation of α-syn or vice versa. All our data together suggest that soluble Aβ42 provides an accessible hydrophobic surface to promote α-syn aggregation which is no longer accessible in mature Aβ42 fibrils.

The extent of α-syn–Aβ42 co-aggregation depends on available Aβ42. The data discussed so far indicate that soluble Aβ42 catalyzes the aggregation of α-syn. To further investigate this mechanism, we performed ThT fluorescence experiments on solutions containing increasing initial concentrations of monomeric α-syn (ranging from 20 to 140 μM) and 2 μM Aβ42 (**Fig. 4a**). We found that, up to 80 μM α-syn, the lag phase of aggregation decreased at increasing concentrations of α-syn. Additionally, the ThT fluorescence increased, suggesting the more fibrils were generated. Above 80 μM α-syn, the aggregation kinetics did not differ significantly which we confirmed by analysis of the t_{50} of these aggregations and compared them to the 1:70 Aβ42:α-syn molar ratio (**Fig 4b**)**.** This result indicates that above a molar ratio of approximately 1:40 (Aβ42: α-syn), Aβ42 does not catalyze additional α-syn aggregation. Furthermore, we confirmed that Aβ42 remains largely oligomeric at each of these α-syn concentrations by native-PAGE and western blotting analysis (**Fig. 4c**).

Discussion

Understanding protein co-aggregation is crucial for developing diagnostic and therapeutic strategies for neurodegenerative diseases. Recently, the identification of LBs in up to 50% of AD patients and Aβ plaques in up to 50% of PD patients has led to research interest on the heterogenous aggregation of these two peptides.

Although it has previously been reported that α-syn aggregation is triggered by Aβ42 (40) and that Aβ42 aggregation is inhibited by α-syn (37), our findings unify the mechanism of this co-aggregation which has previously remained elusive (**Fig. 5**). Here, we report that when Aβ42 and α-syn are co-incubated *in vitro*, homogenous amyloid fibrils of α-syn are formed. We also show that under these conditions, Aβ42 is associated to but not part of the core of α-syn fibrils and mainly in the oligomeric conformation. Additionally, we observed that Aβ42 can nucleate a limited number of α-syn monomers (approximately 40:1 molar ratio in terms of initial monomeric concentrations). This result suggests an upper bound number of α-syn monomers that Aβ42 can nucleate. We hypothesize that this is likely due to the fact that, upon inducing the formation of α-syn fibrils, Aβ42 remains associated to their surface. Thus, Aβ42 is progressively depleted from solution and unable to catalyze further α-syn aggregation. Of note, Aβ42 and α-syn hetero-oligomers have also been previously identified (41-43). As fibrils composed of both proteins have not been identified *in vivo or in vitro*, based on our data we speculate that Aβ42 oligomers and α-syn interact to form hetero-oligomers which likely serve as nucleation sites for the formation of homogenous α-syn fibrils.

It is important to note that α-syn is not normally highly aggregation-prone. In fact, in general, the protein requires the interaction with other biomolecules to aggregate (45-49). Therefore, Aβ42 oligomers triggering α-syn aggregation is not surprising and a similar stochiometric relationship has been reported for α-syn and exosomes (50) and glycosaminoglycans (51).

It is plausible that the interaction of α-syn and Aβ42 drives Aβ42 to form highly stable, possibly off-pathway, oligomers that could have additional toxic effects besides triggering α-syn aggregation (52). We believe triggering the aggregation of α-syn is likely a secondary toxic mechanism of Aβ42 oligomers. While oligomers of Aβ are widely accepted as the neurotoxic species in AD, we show that it is important not to overlook their consequences in other disease contexts.

Materials and Methods

Expression and purification of Aβ42. Purification of Aβ42 was carried out as previously described (44). Briefly, the Aβ42 peptide conjugated with the spider silk domain (known as the fusion protein, 20 kDa) was expressed by heat-shock transformation in BL21 *Escherichia coli* (*E. Coli*). Cells were grown in LB supplemented with kanamycin (50 µg/ml) at 37°C with shaking at 200 rpm until they reached an OD of 0.8 and were then induced overnight with 0.1 mM IPTG at 20°C with shaking at 200 rpm. Cells were collected the following day by centrifugation and the pellet was resuspended in 20 mM Tris-HCl, 8 M Urea, pH 8. The resuspended cells were sonicated on ice for 20 minutes and centrifuged once more to clear cellular debris. The supernatant was filtered using a 0.22 µm filter and loaded onto two HisTrap HP 5 ml columns (Cytiva, Little Chalfont, UK) in tandem that had been pre-equilibrated with 20 mM Tris-HCl, 8 M Urea, pH 8 supplemented with 15 mM imidazole (binding buffer). Following sample application, the columns were washed with several column volumes of binding buffer. The fusion protein was then eluted with 5 column volumes of 20 mM Tris-HCl, 8 M Urea, pH 8 supplemented with 300 mM imidazole (elution buffer). This was then collected and dialyzed overnight against 20 mM Tris-HCl, pH 8. After dialysis, the concentration of the fusion protein was measured using a nanodrop. TEV protease was added to the fusion protein at a 1:15 molar ratio overnight at 4°C. Following this, 7 M Guanidine-HCl was added to the sample and incubated on ice for 2 h before applying the sample on to a Superdex 75 Increase pg 10/600 column (Cytiva, Little Chalfont, UK) pre-equilibrated

with 20 mM phosphate buffer supplemented with 200 μM EDTA, pH 8 for size-exclusion chromatography. Peaks were collected manually. The concentration of monomeric Aβ42 was determined from the chromatogram using the following calculation:

$[(A_{280}/2)/0.2]/1490 \times 1000 \times 1000$

Where 0.2 is the pathlength (cm) of the ATKA Pure (Cytiva, UK), 1490 $M^{-1}cm^{-1}$ is the molecular co-efficient of Aβ42.

The stock concentration was diluted to 2 μM for experiments in 20 mM Phosphate buffer supplemented with 200 μM EDTA, pH 8. For Aβ42 fibrils, monomeric Aβ42 was incubated for 24 h after size- exclusion at 37°C.The fibrils were collected by centrifugation at max speed for 30 min after which the concentration of the supernatant was measured with a Nanodrop (Thermo Fisher Scientific, Waltham, MA, USA). The concentration of the supernatant was subtracted from the initial monomeric Aβ42 concentration to obtain the fibril concentration. These were then diluted to 2 μM for experiments in 20 mM Phosphate buffer supplemented with 200 μM EDTA.

Expression and purification of α-syn.
The pT7-7 α-syn WT plasmid (a gift from Hilal Lashuel, Addgene, Watertown, NY, United States (53)), with codon Y136 mutated from TAT to TAC to prevent cysteine misincorporation, was transformed into BL21-Gold (DE3) competent E. coli (Agilent Technologies, Santa Clara, CA, USA) according to the manufacturer's instructions. Expression of α-syn was induced using 1 mM IPTG at 28°C overnight, ampicillin (100 μg/ml) was included as necessary. The cells were harvested by centrifugation and resuspended in buffer A (20 mM Tris-HCl, 1 mM EDTA, pH 8.0) and protease inhibitors (Roche, Basel, Switzerland). α-Syn was then purified as previously described (54).

ThT fluorescence assays.
20-100 μM α-syn, 2 μM freshly purified monomeric or fibrillar Aβ42 and the two peptides incubated together were prepared with a final concentration of 10 μM ThT dye, gently vortexed and pipetted into non-binding surface black 96-well plates (Greiner Bio-One, Frickenhausen, Austria) in triplicates. The plate was read in a ClarioStar Plus microplate reader (BMG LabTech, Ortenberg, Germany) at 37°C. The excitation and emission wavelength were set to 440nm and 480nm respectively and fluorescent intensity measurements were taken using spiral averaging (3 mm diameter). Buffer only values were subtracted from the sample readings. Readings were taken every 2-5 min. The data were plotted using GraphPad Prism version 9.3.1 for Windows (GraphPad Software, San Diego, CA, United States)

Immunogold labelling and negative stain transmission electron microscopy
Samples were prepared and incubated for 24 h at 37°C before 4 μl were spotted onto a Formvar/Carbon coated 300 mesh copper grids for 1 minute. Excess sample was removed by blotting dry with Whatman filter paper and the grid was allowed to dry to 2 min. Samples for negative stain TEM were then washed with 4 μl water and stained with 4μl 2% w/v uranyl acetate. Samples for immunogold labelling were blocked using normal goat serum—1:10 dilution in PBS+ [1% BSA, 500 ml/L Tween-20, 10 mM Na EDTA, and 0.2 g/L NaN3] for 15 min after which the grids were incubated on a 20 μl drop of primary antibodies—1:10 dilution of 6E10 (Biolegend, San Diego, CA, USA) and anti-αSyn MJFR1

(Abcam, Cambridge, UK) in PBS at room temperature for 2 h. The grids were then washed with PBS+ three times for 2 min and incubated on a 20 ul drop of secondary antibodies conjugated with gold particles (1:20 dilution of anti-mouse and anti-rabbit secondary antibodies conjugated with 10nm and 6nm gold particles respectively, Abcam, Cambridge, UK). Finally, the grids were washed fives with PBS+ and five times with water for 2 min before being stained with 2% w/v uranyl acetate. Grids were imaged on a T12 Spirit electron microscope (Thermo Fisher Scientific (FEI), Hillsboro, OR, USA). Fibril width was measured using Fiji. All data were plotted using GraphPad Prism version 9.3.1 for Windows (GraphPad Software, San Diego, CA, United States).

Dot blotting

Dot blots were carried out on samples that were aggregated in the microplates without ThT at the endpoint of aggregation. Samples were collected and centrifuged at max speed (~17,000 g) for 30 min on a benchtop centrifuge to separate the soluble and insoluble aggregates. 3-5 repeats of each sample were spotted onto 0.45 µM nitrocellulose membrane and blocked in 5% non-fat milk in 0.1% PBS-Tween for 1 h at RT. The membranes were then incubated in primary antibodies (1:1000 dilution in 0.1% PBS-Tween for both anti-α-syn and 6E10) overnight at 4°C under constant shaking. The following day, the membranes were washed three times for 10 min each in 0.1% PBS-Tween. Membranes were then incubated in secondary antibodies conjugated with an AlexaFluor tag (anti-mouse 647 and anti-rabbit 555, diluted 1:2000 and 1:5000 0.1% PBS-Tween, respectively, Thermo Fisher Scientific, Waltham, MA, USA) at room temperature for 1 hour, protected against light. Following three further washes for 10 min each in 0.1% PBS-Tween, the membranes were detected with the appropriate laser using the Typhoon scanner (GE Healthcare, Amersham, UK).

SDS-PAGE and western blotting

Fibrils from the co-incubation sample were collected by centrifugation at max speed for 30 min and the supernatant (S1) was removed and separated from the pellet (P1). The pellet was washed with 50 µl 2% SDS and centrifuged. The supernatant was again removed (S2) and the pellet was resuspended in 50 µl buffer to remove any residual SDS (P2), the pellet was centrifuged, and the supernatant (S3) and pellet were separated (P3) after which the pellet was treated with 50 µl 4 M guanidine hydrochloric acid (G-HCl) for 2 h at RT before SDS-PAGE and western blot analysis. Samples were prepared in 4X LDS sample buffer and 10X reducing agent after which they were boiled at 95°C for 5 min. Samples were then run on 4-12% Bis-Tris NuPAGE gels (Thermo Fisher Scientific, Waltham, MA, USA) and transferred onto a 0.45 µm nitrocellulose membrane for 7 min at 20 V with the i-Blot 2 (Thermo Fisher, Waltham, MA, USA). Blocking, incubation with antibodies and detections were carried out as described above.

Native-PAGE and western blotting.

Samples were prepared and aggregated in 96-well microplates with a non-binding surface for 24 h after which 20 µl of each sample was prepared in native sample buffer and run on Novex Tris-Glycine gels (Thermo Fisher Scientific, Waltham, MA, USA) in native running buffer as per the manufacturer's instructions. The gel was then transferred onto a 0.45 µM nitrocellulose membrane using an iBlot2 (Thermo Fisher Scientific, Waltham, MA, USA) for 7 min at 25 V. The membrane was then blocked, incubated with primary and secondary antibodies, and imaged as described above.

Acknowledgments
We thank UK Research and Innovation (Future Leaders Fellowship MR/S033947/1), the Engineering and Physical Sciences Research Council (grant EP/S023518/1), the Alzheimer's Society, UK (Grant 511) and Alzheimer's Research UK (ARUK-PG2019B-020) for support. RJT was supported by a scholarship by the Department of Chemistry (Imperial College London). We thank Dr Henrik Biverstål (Karolinska Institutet) for providing the expression plasmid for the silk domain-Aβ42 fusion protein and the Electron Microscopy Centre facilities at The Centre of Structural Biology for TEM experiments. We thank Prof. Louise Serpell (University of Sussex) for helpful discussions.

Author Contributions: D.M.V. and F.A.A. designed the research. D.M.V, R.J.T and Y.J performed the experiments. D.M.V and F.A.A. wrote the manuscript. All authors analyzed the data and commented on the manuscript

Competing Interest Statement: The authors declare that the research was conducted in the absence of any commercial or financial relationships that could be construed as a potential conflict of interest.

References

1. F. Chiti, C. M. Dobson, Protein misfolding, functional amyloid, and human disease. *Annu Rev Biochem* **75**, 333-366 (2006).
2. C. M. Dobson, Protein folding and misfolding. *Nature* **426**, 884-890 (2003).
3. M. Vendruscolo, J. Zurdo, C. E. MacPhee, C. M. Dobson, Protein folding and misfolding: a paradigm of self-assembly and regulation in complex biological systems. *Philos Trans A Math Phys Eng Sci* **361**, 1205-1222 (2003).
4. G. F. Chen *et al.*, Amyloid beta: structure, biology and structure-based therapeutic development. *Acta Pharmacol Sin* **38**, 1205-1235 (2017).
5. D. M. Bolduc, D. R. Montagna, M. C. Seghers, M. S. Wolfe, D. J. Selkoe, The amyloid-beta forming tripeptide cleavage mechanism of gamma-secretase. *Elife* **5** (2016).
6. Y. Qi-Takahara *et al.*, Longer forms of amyloid beta protein: implications for the mechanism of intramembrane cleavage by gamma-secretase. *J Neurosci* **25**, 436-445 (2005).
7. M. Takami *et al.*, gamma-Secretase: successive tripeptide and tetrapeptide release from the transmembrane domain of beta-carboxyl terminal fragment. *J Neurosci* **29**, 13042-13052 (2009).
8. I. Benilova, E. Karran, B. De Strooper, The toxic Abeta oligomer and Alzheimer's disease: an emperor in need of clothes. *Nat Neurosci* **15**, 349-357 (2012).
9. C. Haass, D. J. Selkoe, Soluble protein oligomers in neurodegeneration: lessons from the Alzheimer's amyloid beta-peptide. *Nat Rev Mol Cell Biol* **8**, 101-112 (2007).
10. W. Jongbloed *et al.*, Amyloid-beta oligomers relate to cognitive decline in Alzheimer's disease. *J Alzheimers Dis* **45**, 35-43 (2015).
11. C. A. McLean *et al.*, Soluble pool of Abeta amyloid as a determinant of severity of neurodegeneration in Alzheimer's disease. *Ann Neurol* **46**, 860-866 (1999).
12. D. A. Butterfield, D. Boyd-Kimball, Oxidative Stress, Amyloid-beta Peptide, and Altered Key Molecular Pathways in the Pathogenesis and Progression of Alzheimer's Disease. *J Alzheimers Dis* **62**, 1345-1367 (2018).

13. S. M. Butterfield, H. A. Lashuel, Amyloidogenic protein-membrane interactions: mechanistic insight from model systems. *Angew Chem Int Ed Engl* **49**, 5628-5654 (2010).
14. A. Deshpande, E. Mina, C. Glabe, J. Busciglio, Different conformations of amyloid beta induce neurotoxicity by distinct mechanisms in human cortical neurons. *J Neurosci* **26**, 6011-6018 (2006).
15. G. M. Shankar *et al.*, Natural oligomers of the Alzheimer amyloid-beta protein induce reversible synapse loss by modulating an NMDA-type glutamate receptor-dependent signaling pathway. *J Neurosci* **27**, 2866-2875 (2007).
16. G. M. Shankar *et al.*, Amyloid-beta protein dimers isolated directly from Alzheimer's brains impair synaptic plasticity and memory. *Nat Med* **14**, 837-842 (2008).
17. M. Townsend, G. M. Shankar, T. Mehta, D. M. Walsh, D. J. Selkoe, Effects of secreted oligomers of amyloid beta-protein on hippocampal synaptic plasticity: a potent role for trimers. *J Physiol* **572**, 477-492 (2006).
18. P. T. Wong *et al.*, Amyloid-beta membrane binding and permeabilization are distinct processes influenced separately by membrane charge and fluidity. *J Mol Biol* **386**, 81-96 (2009).
19. G. Forloni, C. Balducci, Alzheimer's Disease, Oligomers, and Inflammation. *J Alzheimers Dis* **62**, 1261-1276 (2018).
20. A. Caccamo, A. Magri, S. Oddo, Age-dependent changes in TDP-43 levels in a mouse model of Alzheimer disease are linked to Abeta oligomers accumulation. *Mol Neurodegener* **5**, 51 (2010).
21. R. A. Armstrong, N. J. Cairns, P. L. Lantos, beta-Amyloid (A beta) deposition in the medial temporal lobe of patients with dementia with Lewy bodies. *Neurosci Lett* **227**, 193-196 (1997).
22. T. Bachhuber *et al.*, Inhibition of amyloid-beta plaque formation by alpha-synuclein. *Nat Med* **21**, 802-807 (2015).
23. F. Bassil *et al.*, Amyloid-Beta (Abeta) Plaques Promote Seeding and Spreading of Alpha-Synuclein and Tau in a Mouse Model of Lewy Body Disorders with Abeta Pathology. *Neuron* **105**, 260-275 e266 (2020).
24. R. de Flores *et al.*, Contribution of mixed pathology to medial temporal lobe atrophy in Alzheimer's disease. *Alzheimers Dement* **16**, 843-852 (2020).
25. S. E. Marsh, M. Blurton-Jones, Examining the mechanisms that link beta-amyloid and alpha-synuclein pathologies. *Alzheimers Res Ther* **4**, 11 (2012).
26. Y. H. Shih *et al.*, TDP-43 interacts with amyloid-beta, inhibits fibrillization, and worsens pathology in a model of Alzheimer's disease. *Nat Commun* **11**, 5950 (2020).
27. G. Monzio Compagnoni, A. Di Fonzo, Understanding the pathogenesis of multiple system atrophy: state of the art and future perspectives. *Acta Neuropathol Commun* **7**, 113 (2019).
28. B. A. Silva, L. Breydo, V. N. Uversky, Targeting the chameleon: a focused look at alpha-synuclein and its roles in neurodegeneration. *Mol Neurobiol* **47**, 446-459 (2013).
29. M. G. Spillantini *et al.*, Alpha-synuclein in Lewy bodies. *Nature* **388**, 839-840 (1997).
30. W. R. Galpern, A. E. Lang, Interface between tauopathies and synucleinopathies: a tale of two proteins. *Ann Neurol* **59**, 449-458 (2006).

31. D. J. Irwin, V. M. Lee, J. Q. Trojanowski, Parkinson's disease dementia: convergence of alpha-synuclein, tau and amyloid-beta pathologies. *Nat Rev Neurosci* **14**, 626-636 (2013).
32. R. L. Hamilton, Lewy bodies in Alzheimer's disease: a neuropathological review of 145 cases using alpha-synuclein immunohistochemistry. *Brain Pathol* **10**, 378-384 (2000).
33. K. A. Jellinger, Lewy body-related alpha-synucleinopathy in the aged human brain. *J Neural Transm (Vienna)* **111**, 1219-1235 (2004).
34. P. H. Jensen *et al.*, Binding of Abeta to alpha- and beta-synucleins: identification of segments in alpha-synuclein/NAC precursor that bind Abeta and NAC. *Biochem J* **323 (Pt 2)**, 539-546 (1997).
35. V. Kallhoff, E. Peethumnongsin, H. Zheng, Lack of alpha-synuclein increases amyloid plaque accumulation in a transgenic mouse model of Alzheimer's disease. *Mol Neurodegener* **2**, 6 (2007).
36. K. Ono, R. Takahashi, T. Ikeda, M. Yamada, Cross-seeding effects of amyloid beta-protein and alpha-synuclein. *J Neurochem* **122**, 883-890 (2012).
37. E. Chau, J. R. Kim, alpha-synuclein-assisted oligomerization of beta-amyloid (1-42). *Arch Biochem Biophys* **717**, 109120 (2022).
38. J. Candreva, E. Chau, M. E. Rice, J. R. Kim, Interactions between Soluble Species of beta-Amyloid and alpha-Synuclein Promote Oligomerization while Inhibiting Fibrillization. *Biochemistry* **59**, 425-435 (2020).
39. S. Chia *et al.*, Monomeric and fibrillar alpha-synuclein exert opposite effects on the catalytic cycle that promotes the proliferation of Abeta42 aggregates. *Proc Natl Acad Sci U S A* **114**, 8005-8010 (2017).
40. J. Koppen *et al.*, Amyloid-Beta Peptides Trigger Aggregation of Alpha-Synuclein In Vitro. *Molecules* **25** (2020).
41. M. Iljina *et al.*, Quantifying Co-Oligomer Formation by alpha-Synuclein. *ACS Nano* **12**, 10855-10866 (2018).
42. I. F. Tsigelny *et al.*, Mechanisms of hybrid oligomer formation in the pathogenesis of combined Alzheimer's and Parkinson's diseases. *PLoS One* **3**, e3135 (2008).
43. E. J. Shin, J. W. Park, Nanoaggregates Derived from Amyloid-beta and Alpha-synuclein Characterized by Sequential Quadruple Force Mapping. *Nano Lett* **21**, 3789-3797 (2021).
44. A. Abelein *et al.*, High-yield Production of Amyloid-beta Peptide Enabled by a Customized Spider Silk Domain. *Sci Rep* **10**, 235 (2020).
45. C. Galvagnion *et al.*, Lipid vesicles trigger alpha-synuclein aggregation by stimulating primary nucleation. *Nat Chem Biol* **11**, 229-234 (2015).
46. N. Candelise *et al.*, Effect of the micro-environment on alpha-synuclein conversion and implication in seeded conversion assays. *Transl Neurodegener* **9**, 5 (2020).
47. C. Galvagnion, The Role of Lipids Interacting with alpha-Synuclein in the Pathogenesis of Parkinson's Disease. *J Parkinsons Dis* **7**, 433-450 (2017).
48. M. Grey, S. Linse, H. Nilsson, P. Brundin, E. Sparr, Membrane interaction of alpha-synuclein in different aggregation states. *J Parkinsons Dis* **1**, 359-371 (2011).
49. R. Vacha, S. Linse, M. Lund, Surface effects on aggregation kinetics of amyloidogenic peptides. *J Am Chem Soc* **136**, 11776-11782 (2014).
50. M. Grey *et al.*, Acceleration of alpha-synuclein aggregation by exosomes. *J Biol Chem* **290**, 2969-2982 (2015).

51. S. Mehra *et al.*, Glycosaminoglycans have variable effects on alpha-synuclein aggregation and differentially affect the activities of the resulting amyloid fibrils. *J Biol Chem* **293**, 12975-12991 (2018).
52. A. J. Dear *et al.*, Identification of on- and off-pathway oligomers in amyloid fibril formation. *Chem Sci* **11**, 6236-6247 (2020).
53. K. E. Paleologou *et al.*, Phosphorylation at Ser-129 but not the phosphomimics S129E/D inhibits the fibrillation of alpha-synuclein. *J Biol Chem* **283**, 16895-16905 (2008).
54. W. E. Arter *et al.*, Rapid Structural, Kinetic, and Immunochemical Analysis of Alpha-Synuclein Oligomers in Solution. *Nano Lett* **20**, 8163-8169 (2020).

Figures

Figure 1.

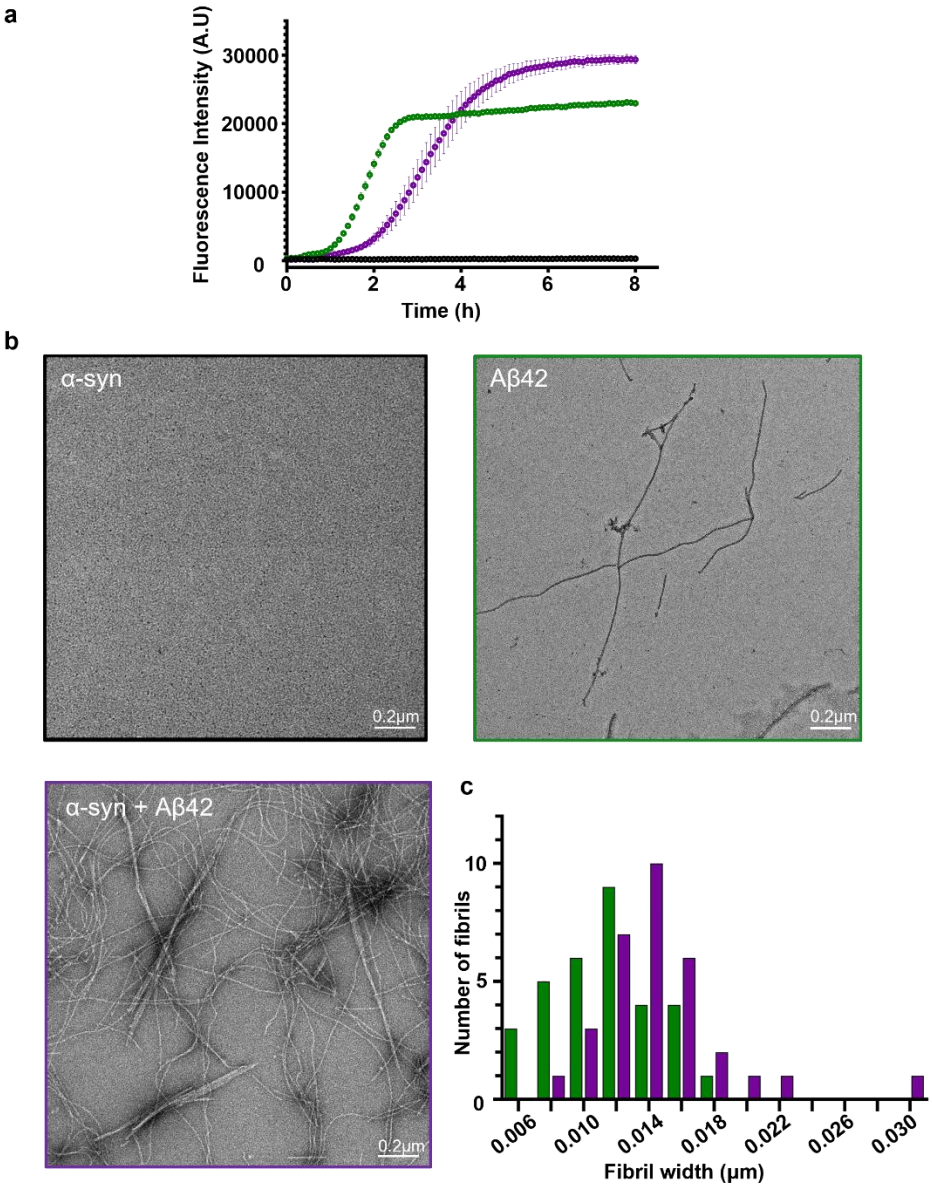

Figure 1. Aggregation of α-syn–Aβ42 co-incubation (a) ThT fluorescence assay of 60 μM α-syn (black), 2 μM Aβ42 (green) and α-syn aggregated with Aβ42 (purple). The average of three replicates for each condition are shown. Error bars represent standard deviation. (b) TEM images of α-syn, Aβ42 and α-syn incubated with Aβ42 at the end of aggregation. No aggregates are seen for α-syn, however, fibrillar aggregates are seen for both Aβ42 and the co-incubated sample. (c) Width distribution of Aβ42 fibrils (black, n = 32) and fibrils in the co-incubation sample (grey, n = 32).

Figure 2.

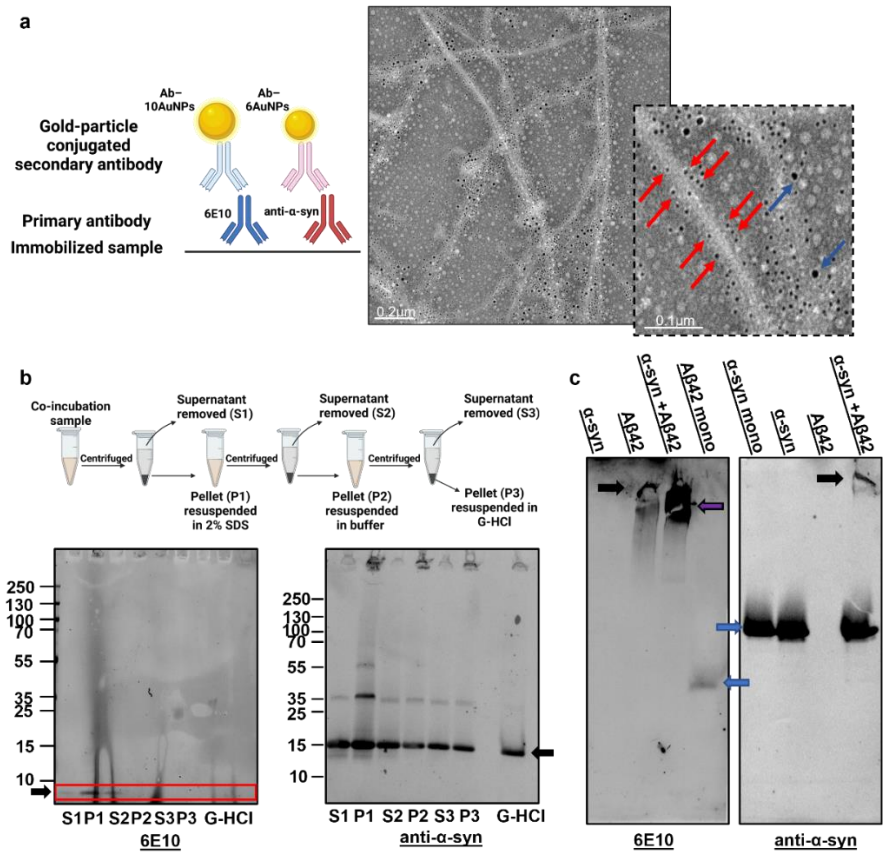

Figure 2. Homogenous α-syn fibrillar aggregates are formed in co-incubation conditions. (a) Immunogold labelling and negative stain electron micrograph α-syn aggregated with Aβ42 at the end point of aggregation. Schematic created on Biorender. Fibrils are highly decorated with 6nm gold particles (Ab–6AuNPs, red arrows) specific for α-syn as opposed to 10nm gold particles labelling Aβ (Ab–10AuNPs, blue arrows) which are sparse. (b) Schematic of G-HCl treatment of SDS insoluble fraction (top) created on Biorender. Fibrils from the co-incubated sample were collected by centrifugation and the supernatant (S1) was removed and separated from the pellet (P1). The pellet was washed with 2% SDS and centrifuged. The supernatant was again removed (S2) and the pellet was resuspended in buffer (P2). The pellet was centrifuged, and the supernatant (S3) and pellet were separated (P3) after which the pellet was treated with 4M G-HCl for 2h at RT before SDS-PAGE and western blot analysis. Detection with the 6E10 antibody (bottom left) revealed no Aβ42 in the G-HCl treated pellet, however, α-syn was detected with the anti-α-syn antibody (bottom right). Monomers of the proteins are indicated by the black arrows (c) Native-PAGE and western blot analysis of total samples after aggregation. Detection with the 6E10 antibody (left) revealed α-syn is not detected by this antibody and Aβ42 ran as a smear of higher molecular weight assemblies and fibrils in the well that could not enter the gel (black arrow). In contrast, Aβ42 in the co-incubation sample ran as higher molecular weight assemblies (purple arrow), as compared to freshly purified monomeric Aβ42 (blue arrow). Detection with the anti-α-syn antibody (right) revealed that after aggregation α-syn is detected as monomers as compared to freshly purified monomeric α-syn (blue arrow) and Aβ42 is not detected by this antibody. In the co-incubation sample however, there are monomers as well as higher molecular weight species and fibrils stuck in the well of the gel (black arrow).

Figure 3

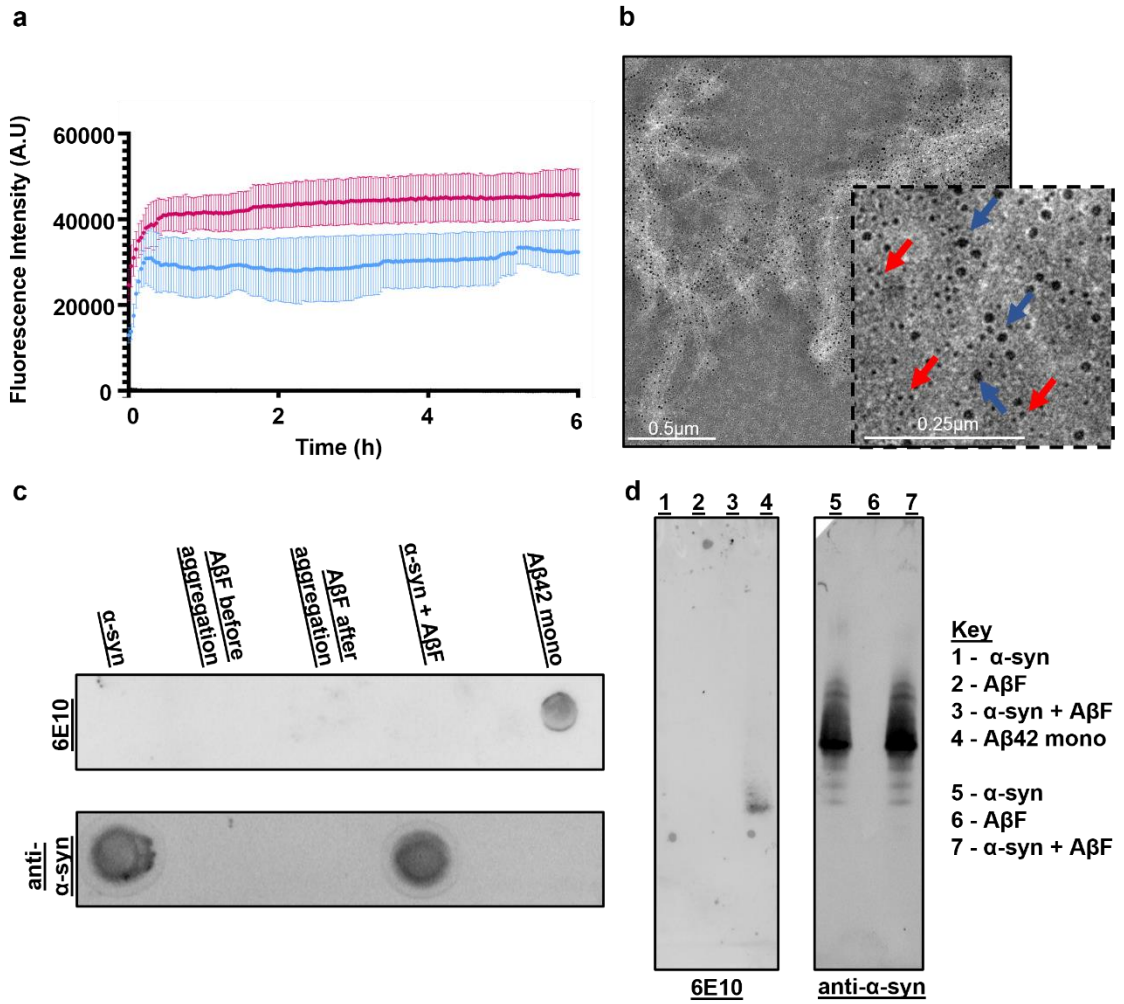

Figure 3. Aβ42 fibrils do not trigger the aggregation of soluble α-syn. (a) ThT fluorescence assay of 60 µM α-syn (black), 2 µM Aβ fibrils (blue) and α-syn aggregated with Aβ fibrils (pink). The average of three replicates for each condition are shown. Error bars represent standard deviation. (b) Immunogold labelling and negative stain TEM of α-syn aggregated with Aβ fibrils at the end point of aggregation. Fibrils are highly decorated with 10nm gold particles (Ab–6AuNPs, red arrows) specific for Aβ42 as opposed to 6nm gold particles labelling α-syn (Ab–10AuNPs, blue arrows) which are largely in the surrounding area of the fibrils. (c) Dot blot analysis on the soluble fractions of aggregated samples detected with 6E10 (top) and anti-α-syn (bottom) primary antibodies. No soluble Aβ42 was detected in any sample except freshly purified Aβ42 monomers as expected and similar intensities of α-syn were detected in the α-syn only and α-syn aggregated with Aβ42 fibrils sample. (d) Native-PAGE and western blot analysis of total samples after aggregation. Detection with 6E10 (left) revealed no detection of (1) α-syn, (2) that Aβ42 fibrils alone do not enter the gel, (3) the co-incubated sample also has no detectable Aβ42 in the gel however (4) freshly purified Aβ42 monomers are detectable. Detection with the anti-α-syn (right) revealed no difference in the molecular weight assemblies of α-syn either (5) alone or (7) aggregated with Aβ42 fibrils. (6) Aβ42 fibrils are not detected by this antibody.

Figure 4.

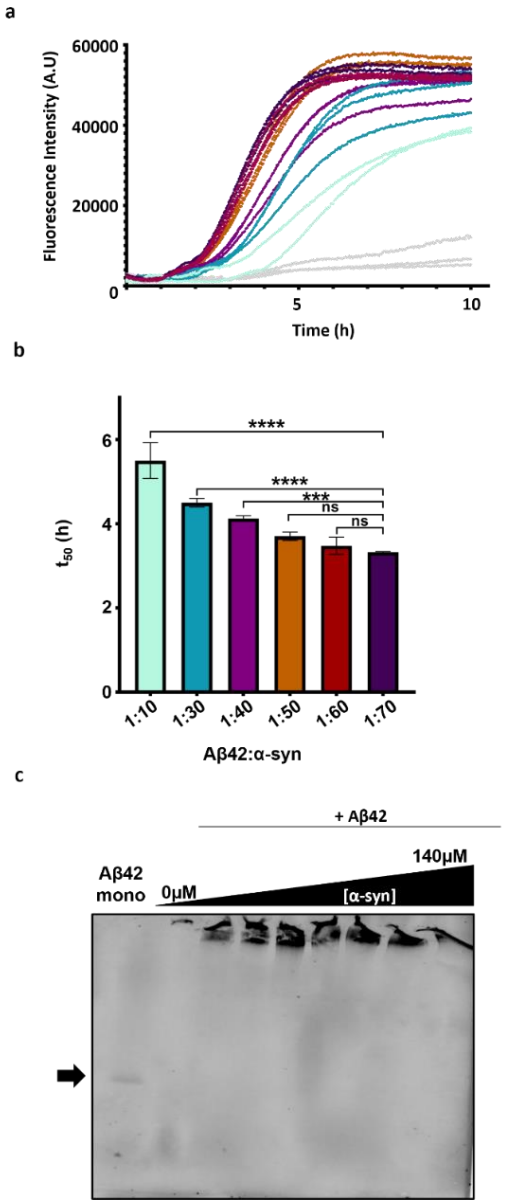

Figure 4. The aggregation in co-incubation conditions is limited by the amount of Aβ42. (a) ThT fluorescence assay of soluble 2 μM Aβ42 with increasing α-syn concentrations (20, 60, 80, 100, 120 and140 μM, light green to dark purple, respectively. 140μM α-syn alone is shown in grey). 2-3 individual replicates are shown for each condition. (b) The half-time of aggregation, t50, was plotted for each molar ratio and compared the 1:70 ratio. There is no significant difference in the t50 of aggregation above a 1:40 Aβ42:α-syn molar ratio suggesting a threshold of Aβ42 catalyzed α-syn aggregation. Error bars are shown as SD. The t50 of aggregations were compared to the 1:70 sample with One-way ANOVA, Dunnett's multiple comparison t-test where p = ≥0.05 (ns), 0.01-0.05 (*), 0.001-0.01 (**), 0.0001-0.001 (***) and <0.0001 (****). (c) Native-PAGE and western blot analysis revealed that compared to monomeric Aβ42, Aβ42 after aggregation was detected only has aggregates stuck in the well of the gel. In the presence of increasing α-syn concentrations of 20-100 μM), Aβ42 remains as soluble high molecular weight assemblies.

Figure 5.

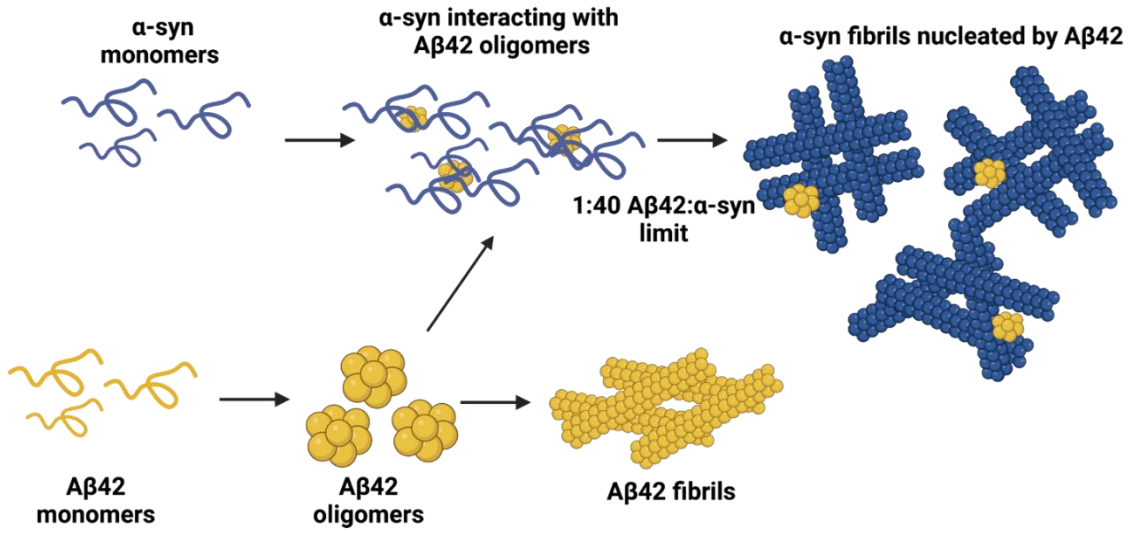

Figure 5. Proposed model for the co-aggregation of Aβ42 and α-syn. When in isolation, Aβ42 undergoes a complete aggregation process that leads to the formation of mature amyloid fibrils. In the presence of α-syn, Aβ42 fibril formation is inhibited. We speculate that, once Aβ42 oligomers are formed, these can interact with α-syn monomers. These heterogenous oligomers serve as nucleation sites for α-syn aggregation and catalyze the formation homogenous α-syn fibrils. The final yield of α-syn fibrils is limited by the amount of Aβ42 and, in our experimental conditions, approximately 40 α-syn monomers per monomer of Aβ42 can form fibrils. Created on Biorender.